Neutron Elastic and Inelastic Cross Section Measurements on Silicon from 0.8 – 8 MeV

A.P.D. Ramirez[a,b], E.E. Peters[a], S. Mukhopadhyay[a,b], M.T. McEllistrem,[b,1], S.W. Yates[a,b], E.C. Derdeyn[d], S.F. Hicks[b,d], E.M. Lyons[d], T.J. Morin[d], J.R. Vanhoy[c]

[a] *Department of Chemistry, University of Kentucky, Lexington, KY 40506-0055, USA*
[b] *Department of Physics and Astronomy, University of Kentucky, Lexington, KY 40506-0055, USA*
[c] *Department of Physics, United States Naval Academy, Annapolis, MD 21402-5026, USA*
[d] *Department of Physics, University of Dallas, Irving, TX 75062-4736, USA*

Abstract

Neutron elastic and inelastic scattering differential cross sections were measured at angles between 30° and 155° with incident neutron energies between 0.8 and 8 MeV. The measured differential scattering cross sections are compared to existing measurements and the ENDF/B-VIII.0, the JEFF-3.3, and the JENDL-4.0 data evaluations, as well as theoretical calculations from the TALYS-1.95 nuclear reaction code. Our results are reasonably well described by values from the ENDF/B-VIII.0 and JEFF-3.3 compilations. However, below 4 MeV, our backward-angle elastic scattering results tend to be lower than database/calculated values, suggesting that less recoil damage would occur than expected. Above 6 MeV, larger backward-angle cross sections are observed suggesting the opposite. Deexcitation γ rays produced in the inelastic scattering process were also studied for neutron energies between 1.9 and 4.5 MeV. Neutron inelastic scattering cross sections deduced from ^{28}Si(n,n$_1\gamma$) γ-ray projection cross sections confirm our ^{28}Si(n,n$_1$) results. To the extent that data from GELINA and our experimental results can be compared, we have excellent agreement between the neutron inelastic scattering cross sections.

Key words: Neutron elastic and inelastic scattering, differential cross sections, ^{nat}Si(n,n$'$), TALYS

---

1. Introduction

As the second most abundant element in the Earth's crust, it is not surprising that silicon has a role in a variety of applications. In nuclear science for example, silicon is present in concrete shielding material, in semiconductor devices such as nuclear radiation detectors, and as fuel and structural materials in advanced fission and fusion reactors. In recent years, silicon carbide (SiC), a composite of silicon, has drawn interest as potential cladding material in accident tolerant fuel that could prevent accidents such as the Fukushima Daiichi power plant incident. Unlike the zirconium alloy used in most water-cooled plants, SiC produces up to a thousand times less hydrogen when reacting with hot steam [1–3]. SiC is also a low-activation material compared to steel alloys. When free from other elements, SiC retains its original mechanical properties better than irradiated steel. However, there is some concern that burnup and displacements of the Si atom in the SiC lattice may cause weakening of the material, and hydrogen could be produced via the (n,p) reaction [4]. Because of these recent developments, SiC and its composites

---

Email addresses: `ramirez112@llnl.gov` (A.P.D. Ramirez), `hicks@udallas.edu` (S.F. Hicks), `vanhoy@usna.edu` (J.R. Vanhoy)

[1] Deceased

have gained appreciable attention in both computational modeling and experimental measurements to study the effects of neutron irradiation on these materials. Therefore, it is necessary to have accurate knowledge of neutron scattering cross sections for silicon and carbon to evaluate the behavior of these materials under extreme conditions.

In this work, we present new neutron elastic and inelastic scattering differential cross sections on natural silicon for incident energies between 0.8 and 8.0 MeV. These data are also complemented with γ-ray production cross sections from low-lying transitions of the stable isotopes of silicon for neutron energies between 1.9 and 4.5 MeV. These data are compared with evaluation libraries [5–7], which are commonly used cross section databases to study radiation transport and material damage for advanced nuclear applications, previously reported data [8–24], and predictions from theoretical calculations from the TALYS-1.95 nuclear reaction code [25]. The paper is organized as follows: an overview of our experimental techniques and data analysis procedure are given in Section 2; the discussion of our results and comparisons with previously reported data, evaluation databases, and theoretical calculations are presented in Section 3; finally, a summary of our main results is found in Section 4.

2. Experimental Methods

The University of Kentucky Accelerator Laboratory (UKAL) features a 7 MV single-ended model CN Van de Graaff accelerator with a terminal-based bunching system. Neutrons were produced via the ^{3}H(p,n)^{3}He and ^{2}H(d,n)^{3}He reactions for energies below and above 4.5 MeV, respectively. The tritium or deuterium gas was contained in 3-cm-long stainless-steel cell assembly attached to the end of the beam line. The cell had a tantalum liner and button to prevent neutron production in the stainless steel. A molybdenum foil of 3.3 μm thickness was used to separate the beam-line vacuum from the approximately 1 atm of deuterium or tritium gas in the cell. The pulsed beam delivered to the gas cell had a repetition rate of 1.875 MHz and a time spread of about 1 ns. The full width at half maximum (FWHM) of the neutron energies emitted at 0° was approximately 80 keV at 3.5 MeV and 175 keV at 6.0 MeV calculated from the time width of the beam pulse, the energy loss of the beam in the gas cell, and the energy spread of neutrons over the extended sample; the energy straggling in the foil was also taken into account. The equipment, laboratory, methods, and data reduction techniques are presented in Refs. [26–30].

Neutrons produced in the gas cell assembly were monitored by NE213 and C_6D_6 liquid scintillation detectors as forward monitors (FM). One of the FM detectors was positioned at 45° with respect to the incident beam direction to provide a direct and collimated view of the gas cell during the measurements. When using the ^{2}H(d,n)^{3}He reaction, a second FM detector was set at 20° due to the low neutron production cross sections at 45°. In addition to the forward monitors, a long counter composed of a BF_3 proportional counter surrounded by polyethylene and paraffin wax was placed 4 m away from the gas cell at 90° relative to the incident beam direction. The number of neutrons recorded by these detectors is directly proportional to the fluence out of the gas cell.

Cylindrical scattering samples were suspended about 8 cm away from the center of the gas cell at 0° relative to the direction of the incident beam. The primary scattering sample was 7.3 g of high-purity natural silicon with dimensions 1.58 cm × 1.57 cm (diameter × height). A polyethylene solid cylinder with dimensions 0.96 cm × 1.49 cm (diameter × height) was used to measure the ^{1}H(n,n)^{1}H cross sections for the absolute normalization of our (n,n$'$) data. Additionally, enriched ^{56}Fe (99.87% ^{56}Fe) and ^{nat}Ti cylindrical scattering samples with dimensions 1.52 cm × 1.45 cm and 2.23 cm × 2.55 cm (diameter × height), respectively, were employed for absolute normalization of our neutron scattering cross sections deduced from our γ-ray production cross sections. Further discussion of the normalization procedure is provided below.

The MAIN neutron detector used to register scattered neutrons was a C_6D_6 liquid scintillation detector. It was positioned on a carriage that is rotatable about its pivot point directly under the center of the scattering sample and from 0° to 155° with respect to the incident beam direction. The carriage supports a full-length collimation system composed of layers of tungsten, copper, lead, and boron-loaded hydrocarbon accommodating flight paths up to 4 m. On-pulse neutrons were identified by time-of-flight (TOF) and pulse-shape discrimination (PSD) techniques. An example of a background-subtracted TOF spectrum illustrating the resolved elastic and inelastic peaks from neutrons scattered from the ^{nat}Si sample is shown in Fig. 1. This TOF spectrum was generated by taking the difference between the target-in (with scattering sample) and the target-out (without scattering sample) spectra where the latter accounts for room-scattered neutrons.

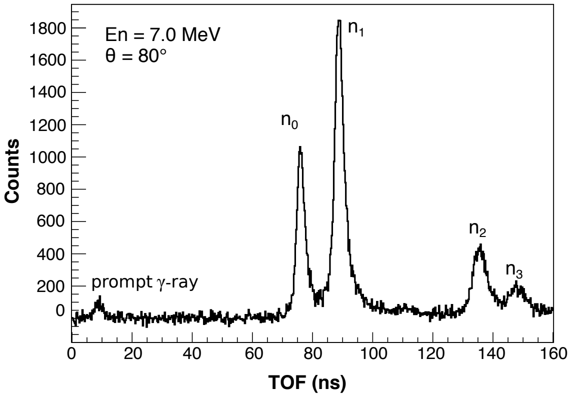

Figure 1: A background-subtracted neutron TOF spectrum for ^{nat}Si(n,n$'$)^{nat}Si with $E_n = 7.0$ MeV at $\theta = 80°$. The peak on the left is from leakage of prompt γ rays through the PSD, and the other peaks are the elastic and inelastic neutron peaks.

The efficiency of the MAIN detector was measured from the neutron angular distribution of the source reaction in the gas cell. The efficiency was determined by taking the ratio of the neutron counts, normalized by the neutron fluence, and the known source reaction cross sections, $d\sigma/d\Omega_{(Tpn/Ddn)}$, taken from the DROSG-2000 neutron source reaction program [31, 32]. Since the relative detection efficiency was used in the differential cross section determination, we only considered the angular dependence of the source reaction cross sections and not the absolute magnitude. The relative uncertainty of the neutron detector efficiency is approximately 3%.

The (n,n$'$) measurements must be corrected for attenuation and multiple scattering of the incident and exiting neutrons. Attenuation depends on the total cross section at each energy, while multiple scattering depends strongly upon the elastic differential cross section. The MULCAT code handles the combined effect [33] including the experimental geometry. At $E_n = 4.0$ MeV, for detector angles between 30° and 150°, the attenuation causes a 14-15% reduction in detected yield, while multiple scattering causes a 3-18% increase in detected yield in the elastic exit channel. The multiple scattering correction variation for the inelastic exit channel is smaller, 12-18%. The uncertainty in this method is <5% [28].

To convert our data to absolute cross sections, we applied a scaling factor obtained by comparing our n-p scattering data with standard values. The n-p angular distribution was a supplementary measurement performed using the polyethylene sample described earlier to scatter neutrons from protons at five different angles between 30° and 45°. The standard values for the ^{1}H(n,n)^{1}H total cross sections were taken from Refs. [35] and [36]. As the standard values of the differential cross sections in the center-of-mass system (CM) vary only by 0.5% from the isotropic estimate, we assumed that the $d\sigma/d\Omega_{(Hnn)}$ was isotropic in the CM frame.

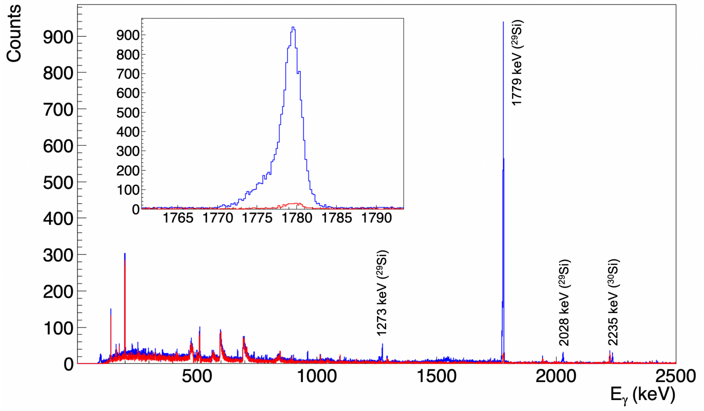

Figure 2: Typical prompt (blue) and background (red) γ-ray spectra for ^{nat}Si(n,n$'\gamma$)^{nat}Si with E_n = 4.0 MeV at θ = 125°. Visible peaks due to other silicon isotopes are highlighted. Additional peaks are from background and neutron-induced events in the detector. The inset shows the expanded prompt and background spectra for the 1779 keV peak.

The deexcitation γ rays following neutron inelastic scattering in the ^{nat}Si sample were also investigated using high-resolution γ-ray spectroscopy. The advantage of γ-ray detection is that peaks are well separated, especially for closely-spaced peaks which are typically difficult to resolve with TOF neutron detection. Comprehensive information about the experimental procedures and analysis techniques for γ-ray measurements at UKAL have been described in Refs. [28, 30]. Here, we briefly mention the methods employed in the present experiments.

The emitted γ rays were recorded with an HPGe detector actively shielded with a BGO annular detector for Compton suppression. The detectors were housed in the shielding and collimation system described earlier for the C_6D_6 MAIN neutron detector modified for the shortened flight path of approximately 130 cm from the scattering sample to the face of the HPGe detector. Using TOF techniques, we further reduced the background events due to scattered neutrons and secondary γ rays that were random in time by applying a gate on the prompt γ-ray peak in the TOF spectrum. Similarly, an off-prompt gate was applied to obtain the background spectrum. We also utilized this off-prompt gate to estimate the contribution to the 1779 keV γ-ray yield from the β decay of ^{28}Al back to ^{28}Si with a 2.25 min half-life produced from the ^{27}Al(n,γ)^{28}Al reaction. Another source of 1779 keV γ rays is the ^{28}Si(n,p)^{28}Al channel which has a threshold at E_n = 4.0 MeV. An example of the γ-ray spectra produced from the neutron inelastic scattering from ^{nat}Si is given in Fig. 2.

The γ-ray production cross sections were determined from the peak yields of the γ rays of interest. Uncertainties due to counting statistics were <7%, with those for E_γ=1779 keV typically <1%. The γ-ray yields were corrected for detector efficiency, neutron multiple scattering, γ-ray attenuation, and neutron fluence in the scattering sample. The relative HPGe detector efficiency was obtained from standard ^{226}Ra and ^{152}Eu sources positioned at the location of the scattering sample. The uncertainty due to the detector efficiency is <2.5%. The (n,n$'\gamma$) measurements must be corrected for attenuation and multiple scattering of the incident neutron and the attenuation of the exiting photon. The program GAMBIT, using the Engelbrecht approach [37, 38] handles the combined effects, including the experimental geometry. For the 1779 keV γ-ray of ^{28}Si, the combined effects are a 10-15% correction for incident neutron energies from 1.9 to 4.0 MeV. The uncertainty in the Engelbrecht method is <4%. For monitoring the neutron fluence, we employed the BF_3 long counter with relatively uniform efficiency curve in the neutron energy region of interest. As the long counter was not positioned at 0°, its yield was also corrected for the angular dependence of the ^{3}H(p,n)^{3}He reaction employing reference values from the DROSG-2000 neutron source reaction program [31, 32]. Finally, to convert the excitation function data to absolute cross sections, we performed additional neutron inelastic scattering measurements for ^{56}Fe and ^{nat}Ti. Specifically, we utilized the γ-ray production cross sections of the 847, 1238, and 1810 keV lines in ^{56}Fe and 984, 1312, and 1437 keV lines in ^{48}Ti with similar incident neutron energies used in ^{nat}Si. The experimental values were then compared with data from Refs. [39] and [40], respectively, as reference values to determine the absolute normalization factor. The latter agrees well with recent measurements from Ref. [41] and evaluation for the 983 keV transition from Ref. [42] with neutron energies below 4.5 MeV.

3. Results and Discussion

3.1. Neutron Detection

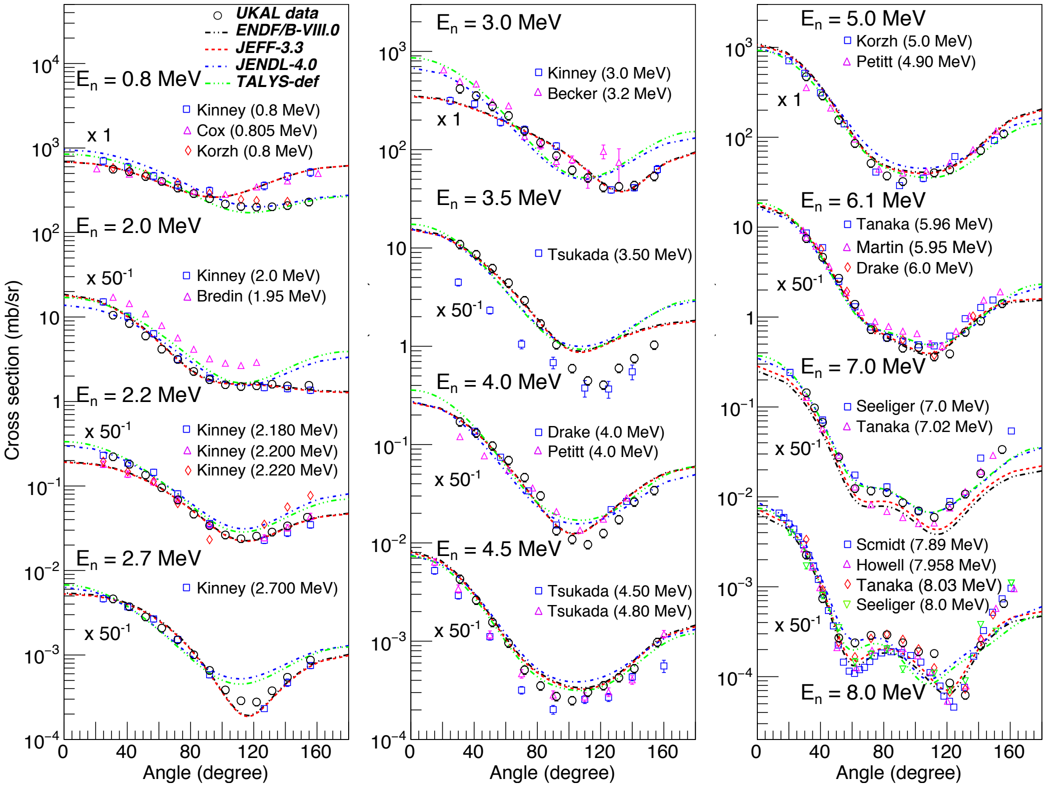

Figure 3: Neutron elastic scattering differential cross sections for ^{nat}Si (open circle) compared with previously reported data [8–22], predictions from the evaluation databases (curves) from ENDF/B-VIII.0 [5] (black), JEFF-3.3 [7](red), and JENDL-4.0 [6] (blue), and theoretical calculations from the TALYS-1.95 code using default parameters [25] (green).

Neutron scattering differential cross section measurements were carried out at 12 incident energies between 0.8 and 8.0 MeV covering the angles from 30° to 155°. The measured elastic angular distributions compared with values from the ENDF/B-VIII.0 [5], the JENDL-4.0 [6] and the JEFF-3.3 [7] evaluation libraries, theoretical calculations using the TALYS-1.95 nuclear reaction program [25], and literature data are shown in Fig. 3. As the scattering sample used in the experiments was elemental, the evaluated ^{nat}Si neutron elastic cross sections were calculated from the sum of the neutron cross sections of ^{28}Si, ^{29}Si, and ^{30}Si weighted according to their natural abundances. The previously reported cross sections were retrieved from the experimental nuclear reaction data (EXFOR) database [43]. The cross sections presented here are all given in the CM frame.

The agreement between our neutron elastic differential cross sections with evaluation databases and previously reported data is adequate, especially at forward angles. A few of the experimental cross sections vary at backward angles while a couple deviate in terms of overall magnitude. For $E_n \geq 7$ MeV, experimental data from different measurements show discrepancies around the middle angles where our data are slightly larger than those from previous experiments. Some of these observed discrepancies may be attributed to incident neutron energy shifts of a few tens of keV or different neutron energy resolution between measurements. In light nuclei such as silicon, scattering cross sections are characterized by resonances associated with large fluctuations in the cross section usually found at low energies. Based on the ENDF/B-VIII.0 evaluation, n-^{28}Si cross sections still show strong resonance fluctuations below 10 MeV, whereas those with known resonance parameters are available only up to $E_n \sim 1.8$ MeV [44, 45].

When compared with evaluation databases, our elastic cross section data tend to favor the ENDF/B-VIII.0 and JEFF-3.3 evaluations. Although, for $E_n \geq 7$ MeV, these evaluated values slightly underestimate the present data at forward angles. Additionally, while different experimental elastic cross section data seem to be in good agreement with each other at the most backward angles in this energy region, the evaluations underestimate these values. This trend continues a little beyond 8 MeV using literature data from Refs. [20, 21]. Below 4 MeV, our backward-angle elastic scattering results tend to be lower than database values.

The comparisons between our neutron inelastic differential cross sections populating the first excited state of ^{28}Si, literature data, and evaluated data are presented in Fig. 4. Our values were corrected for the 92.223% abundance of ^{28}Si in the scattering sample. Most of the experimental cross sections display fair agreement with previously reported data. As with the elastic cross sections, some of the reported data presented here have slightly different incident neutron energies than ours, and this discrepancy may explain the noticeable disagreements. The neutron inelastic scattering cross sections due to scattering to the second and third excited states of ^{28}Si at 4618 keV and 4980 keV, respectively, will not be reported in this paper due to contamination originating from the d+^{16}O and the d+^{12}C reactions in the neutron production cell. Although lower in neutron energies, these contaminant neutrons when elastically scattered from silicon overlap with the higher inelastic peaks of ^{28}Si.

The elastic and inelastic angular distributions can be described in terms of the Legendre polynomial series $\frac{d\sigma}{d\Omega} = \sum_{l=0}^{N} a_l P_l(cos\theta)$ where P_l is the Legendre polynomial of order l and a_l is its coefficient. From the least-squares fits to the data, we obtained the angle-integrated cross sections as shown in Fig. 5 along with values from the evaluation libraries. Because of the narrow fluctuations in the cross sections, we averaged the evaluated data over a 100 keV energy interval to make the resolution comparable to our moderate experimental neutron energy

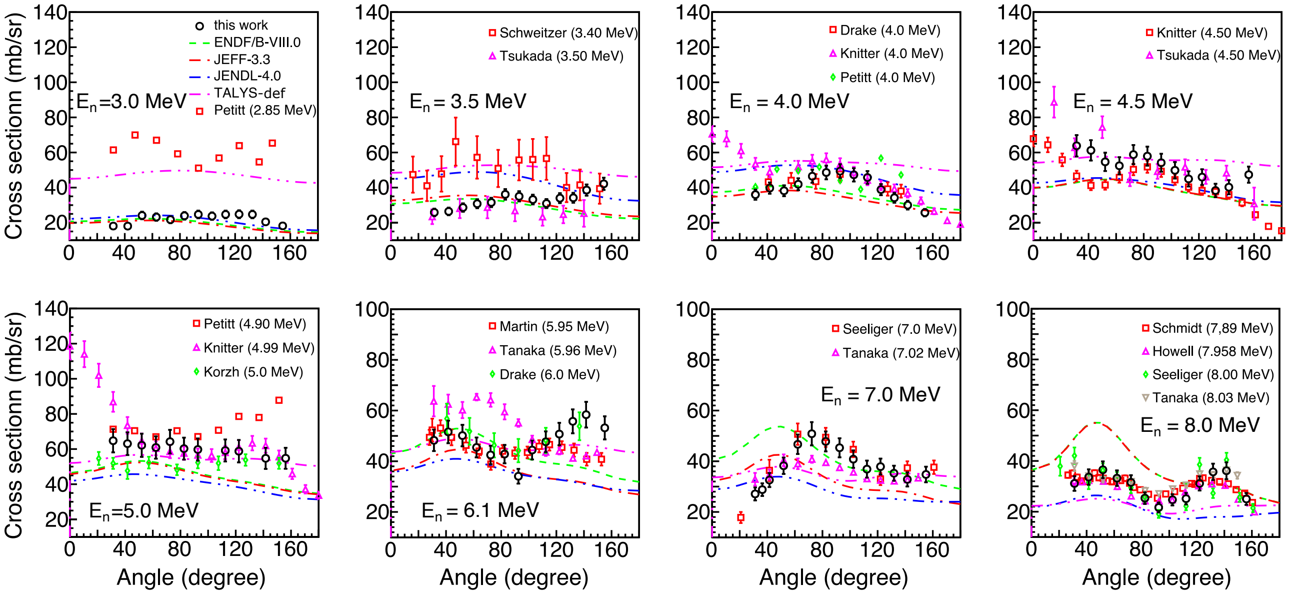

Figure 4: Neutron inelastic differential cross sections for ^{28}Si populating the 1779 keV level (open circle) compared with previously reported data [10, 13, 14, 16–24], predictions from evaluation databases from ENDF/B-VIII.0 [5] (black), JEFF-3.3 [7] (red), and JENDL-4.0 [6] (blue), and theoretical calculations from the TALYS-1.95 code using default parameters [25] (green).

spread. The uncertainties in the cross sections were determined from the uncertainties of the a_0 fit parameter, while the uncertainties in the incident neutron energies were calculated from the width of the beam pulse and the energy spread due to the gas target assembly. Our experimental data follow the ENDF/B-VIII.0 and JEFF-3.3 averaged values rather well.

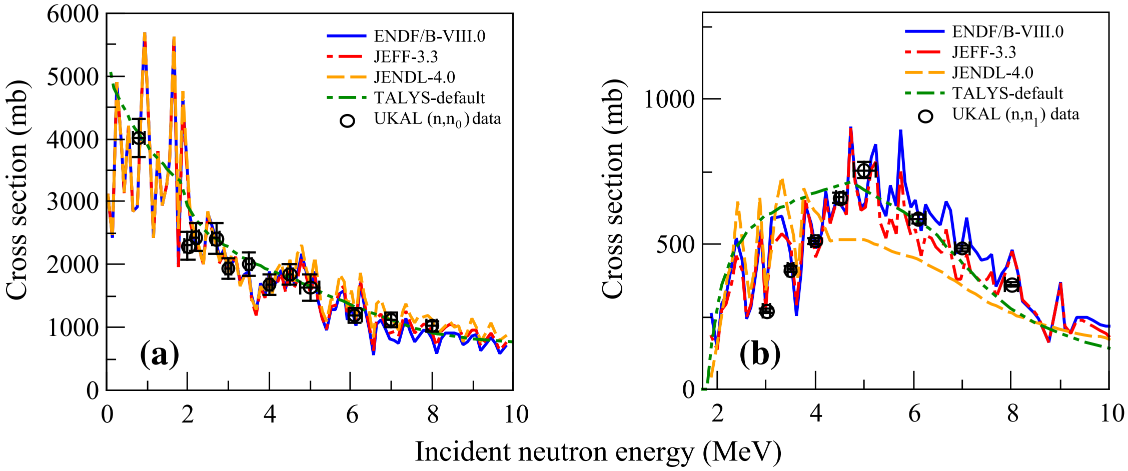

Figure 5: Angle-integrated neutron elastic cross sections for ^{nat}Si (a) and ^{28}Si (E$_\gamma$=1779 keV) (b) cross sections compared with the ENDF/B-VIII.0, JEFF-3.3 and JENDL-4.0 evaluations and TALYS-1.95 calculations.

We further compared the present data with predictions based on the TALYS-1.95 nuclear reaction code employing the default parameter settings. Despite the known strong resonances in the neutron-^{nat}Si cross sections, theoretical values calculated using the TALYS-1.95 code are in good agreement overall with our angle-integrated elastic cross sections as shown in Fig. 5(a). This success is due to the fair description of the predicted elastic scattering differential cross sections of the present data at forward angles, although, underestimation of the backward-angle cross sections is also visible (see Fig. 3). For the inelastic cross sections, however, large discrepancies between the experimental data points and the TALYS values are noticeable, especially at $E_n < 5$ MeV where most of our data points fall into the cross section minimum based on the ENDF/B-VIII.0 evaluated data (see Fig. 5(b)).

3.2. γ-ray Detection

We also investigated the excitation functions and angular distributions of γ rays accompanying neutron inelastic scattering from ^{nat}Si. For the excitation function measurements, emitted γ rays were detected at an angle of 125° relative to the incident beam direction for neutron energies from 1.9 to 4.5 MeV in 100 keV steps. Additionally, γ-ray angular distributions covering about 10 angles between 30° and 150° for 8 incident neutron energies below 4 MeV were measured. For ^{28}Si, only the $E_\gamma = 1779$ keV γ ray from the $2_1^+ \rightarrow 0_{gs}^+$ transition is observed below 4.5 MeV. The angular distribution for this γ ray can be expressed as $W(\theta_\gamma) = A_0\{1 + a_2 P_2(\theta_\gamma) + a_4 P_4(\theta_\gamma)\}$, where P_l's are the Legendre polynomials. The coefficient A_0 is proportional to the γ-ray yield and was used to determine the γ-ray production cross section, while the a_2 and a_4 parameters describe the angular distribution anisotropy. The absence of transitions feeding the first excited state of ^{28}Si below 4.5 MeV means that the 1779 keV production cross section also corresponds to the ^{28}Si(n,n$_1$)^{28}Si level cross section in this incident energy range.

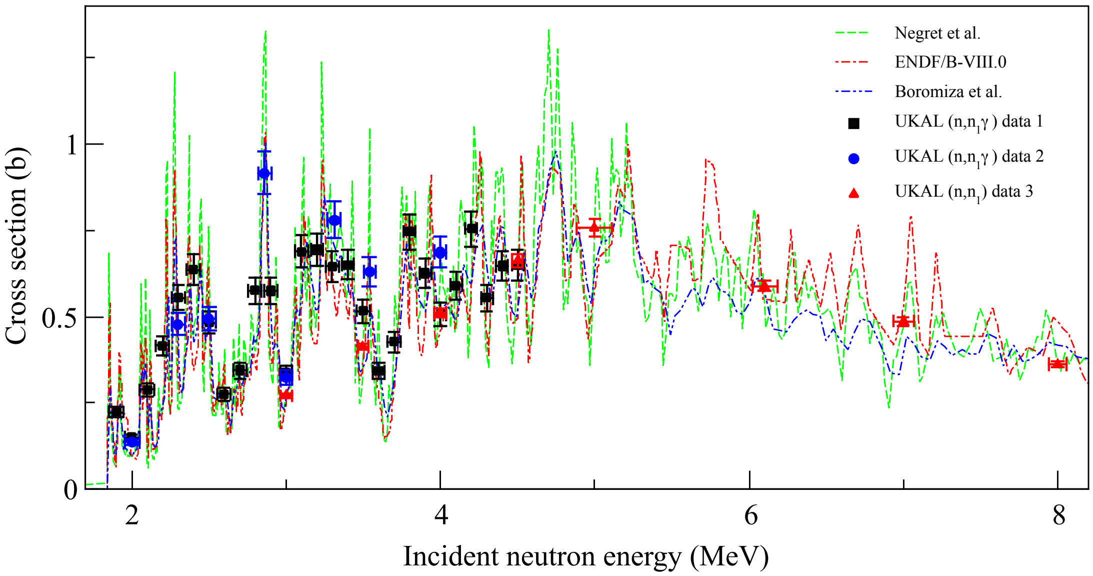

Figure 6: Experimental ^{28}Si(n,n$_1$) cross sections from γ-ray and neutron detection (points) compared with ENDF/B-VIII.0 evaluations (orange line) and recent high-resolution experimental data from Negret et al. [46] (green) and Boromiza et al.[47] (blue). See text for an explanation of the different UKAL data sets.

Fig. 6 displays our ^{28}Si(n,n$_1\gamma$)^{28}Si cross sections for both γ-ray and neutron detection together with values from the ENDF/B-VIII.0 library and the recent high-resolution data by Negret et al. [46] and Boromiza et al. [47] both measured at the GELINA facility. It is worth noting that, even though the GELINA data are generally in good agreement with each other, the Negret et al. [46] data, who used a ^{nat}Si sample similar to the present work, exhibit more fine structure resonances with larger amplitude than the data from Boromiza et al. [47], who used a SiO_2 sample. As for the present work, we provide three inelastic cross section data sets: (1) “UKAL data 1” are γ-ray production cross sections measured at 125°; (2) “UKAL data 2” are γ-ray production cross sections deduced from angular distribution measurements; and (3) “UKAL data 3” are neutron-detection cross sections explained in the previous section. Example neutron inelastic scattering angular distributions from the 1779 keV first excited state of ^{28}Si are shown in Fig. 7.

Excellent agreement between our ^{28}Si(n,n$_1\gamma$) data, ENDF/VIII.0 values, and GELINA data [46, 47] for E_n's below 4.5 MeV is observed. Despite our moderate energy resolution, the global features of the resonances clearly follow the results of Negret et al. [46] in our energy range. In addition, our γ-ray detection data support our neutron-detection results in this energy region. The a_2 and a_4 parameters from “UKAL data 2”, as well as the angle-integrated cross sections are given in Table 1. For E_n = 2.0, 2.5, and 3.0 MeV, “UKAL data 2” with $a_4 <$ 0.05 agree with “UKAL data 1” cross sections within the quoted total uncertainties. While for E_n = 2.30 and 3.31 MeV, “UKAL data 2” with $a_4 >$ 0.1 differ by at least 10% relative to “UKAL data 2”. For E_n = 2.86 and 3.54 MeV, the centroid energies are located at a resonance resulting in a sharp increase in cross sections.

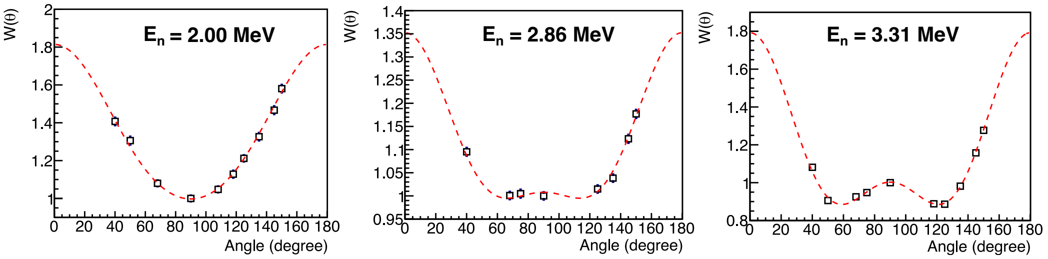

Figure 7: Example angular distributions of the prompt E_γ=1779 keV γ ray measured at selected neutron energies. Only statistical uncertainties are shown and are about the same magnitude or smaller than the data points.The dashed lines are fits of even Legendre polynomials up to order 4.

Table 1: Angle-integrated cross sections for E_γ = 1779 keV measured with the detector at 125° only ”UKAL data 1” and with an angular distribution ”UKAL data 2”. The a_2 and a_4 parameters were obtained from “UKAL data 2”. Data with ^{a}, ^{b} and ^{c} were measured at neutron energies of 2.9, 3.3, and 3.5 MeV, respectively.

Incident neutron energy (MeV)	a_2	a_4	UKAL data 1 (mb)	UKAL data 2 (mb)	UKAL data 3 (mb)
2.0	0.421(17)	0.048(24)	149(10)	138(9)	
2.3	0.372(14)	-0.116(21)	555(37)	478(32)	
2.5	0.292(12)	0.010(16)	483(33)	495(33)	
2.86	0.172(11)	0.109(16)	^{a}575(41)	915(61)	
3.0	0.197(12)	0.019(18)	337(23)	325(22)	271(6)
3.31	0.353(12)	0.370(16)	^{b}645(44)	780(52)	
3.54	0.245(11)	0.010(16)	^{c}516(35)	629(42)	^{c}413(10)
4.0	0.305(20)	0.128(28)	507(34)	687(46)	511(12)

Because our silicon scattering sample was elemental, several of the low-lying γ rays from the neutron inelastic scattering of ^{29}Si (4.685 %) and ^{30}Si (3.092 %) were observed in our γ-ray spectra, as shown in Fig. 2. As their abundances are low, the typical counting statistics of the yields from these γ rays range from 2% - 7%. Previously reported γ-ray production cross sections from these isotopes are scarce. Below 10 MeV, the EXFOR [43] database only has the previously reported data from Drake et al. [14], Lind et al. [48], and Schmidt et al. [21]. We use the former two data sets for comparison with this work.

Fig. 8 shows our measured γ-ray production cross sections for the 1273 and 2028 keV γ rays from n-^{29}Si and the 2235 keV γ ray from n-^{30}Si compared to literature data from Drake et al. [14] and Lind et al. [48], as well as theoretical calculations based on the TALYS-1.95 reaction code. The data from Drake et al. [14] have been reported as elemental cross sections and were, hence, corrected according to the isotopic abundances; the data from Lind et al. [48] do not contain uncertainties. Our 2028- and 2235-keV γ-ray production cross sections are consistent with those from Lind et al.[48], except for the 1273 keV γ ray for which Lind et al. [48] have drastically smaller values. It was noted in Ref. [48], however, that the measurement was performed using a NaI detector with a relatively poor γ-ray resolution making it difficult to properly separate the 1273 keV peak with the single escape peak from the dominant 1779 keV γ ray. The data from Drake et al. [14] also agree with our values at 4.0 MeV, although their data have relatively large uncertainties. There is also a noticeable fluctuation in the experimental cross sections, which is suggestive of resonance structures similar to ^{28}Si. In terms of the overall magnitude, the TALYS-1.95 predicted production cross sections agree fairly well for the experimental n-^{29}Si production cross sections, but the calculations slightly overestimate the n-^{30}Si data.

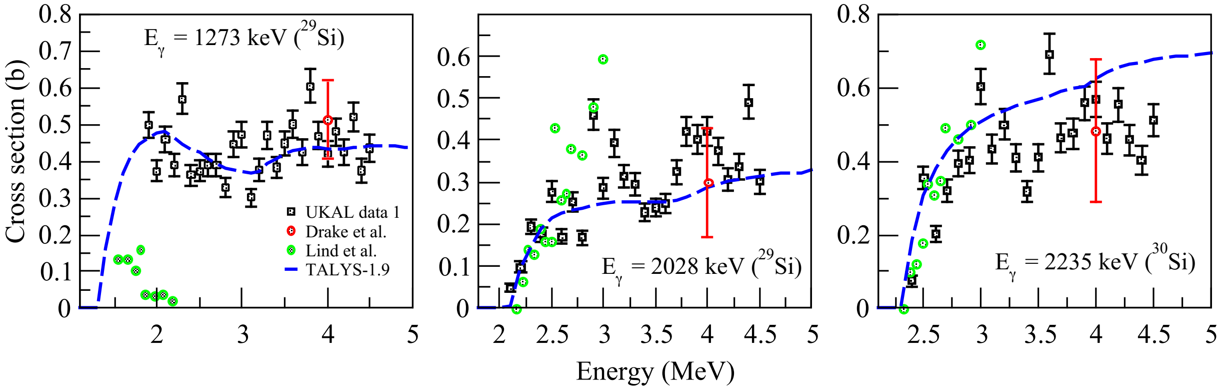

Figure 8: Experimental γ-ray production cross sections for the low-lying γ rays in ^{29}Si and ^{30}Si compared with reported data from Refs. [14, 48] and predictions from the TALYS-1.95 code.

4. Summary

In summary, neutron elastic and inelastic scattering differential cross sections were measured at 12 incident energies between 0.8 and 8 MeV on natural silicon. The comparison of our data with literature values shows reasonable agreement for the elastic scattering cross sections but noticeable deviations appear for the ^{28}Si(n,n$_1$)^{28}Si cross sections. This disagreement may be attributed to slight differences in experimental incident neutron energy, as well as energy resolution, which could influence measured cross sections that feature strong resonance structures such as for silicon. Below 4 MeV, some of our cross sections tend to be smaller than the evaluated database values at large-angle scattering, suggesting less recoil damage than expected, while above 6 MeV, we observe the opposite. For the angle-integrated cross sections, our data are in good agreement with evaluated data from ENDF/B-VIII.0 and JEFF-3.3 except for a couple of high neutron energy cross sections, which differ beyond our quoted uncertainties.

We also report γ-ray production cross sections for ^{28}Si measured from 1.9 to 4.5 MeV. These data were compared with our (n,n$_1$) cross sections, evaluated data, and the recent high-resolution measurements at GELINA from Refs. [46, 47]. Excellent agreement among these data sets was observed. The large amplitude resonance structures reported in Ref. [46] seem to be supported by our data in the energy region being studied. The γ-ray production cross sections for the low-lying transitions in ^{29,30}Si have also been presented. The lack of available data for these isotopes prompted us to report these cross sections despite their low statistical quality ($<$7%). Similar to results for ^{28}Si, fluctuations in the cross sections associated with resonance structures have been observed.

5. Acknowledgments

Research at the University of Kentucky Accelerator Laboratory is supported by contracts from the U.S. Department of Energy NNSA-SSAP award NA-0002031 and Nuclear Energy Universities Program award NU-12-KY-UK-0201-05, the Donald A. Cowan Physics Fund at the University of Dallas, and in part by the National Science Foundation grant PHY-1913028. Isotope(s) used in this research were supplied by the U.S. Department of Energy Isotope Program, managed by the Office of Isotope R&D and Production. The authors also acknowledge the many contributions of H.E. Baber to these measurements.

References

[1] L.W. Weston and D.C. Larson. Compilation of requests for nuclear data. United States: N. p., 1993. Web. doi:10.2172/6806265.

[2] P. Hosemann, J.N. Martos, D. Frazer, G. Vasudevamurthy, T.S. Byun, J.D. Hunn, B.C. Jolly, K. Terrani, M. Okuniewski, Journal of Nuclear Materials **442**, 133 (2013).

[3] W. Jiang, J.D.Hales, B.W. Spencer, B.P.Collin, A.E. Slaughter, S.R. Novascone, A. Toptan, K.A. Gamble, R. Gardner, Journal of Nuclear Materials **548**, 152795 (2021).

[4] A. Ivekovi, S. Novak, G. Drai et al., Journal of the European Ceramic Society **33 (10)** pp. 1577-1589 (2013).

[5] M. B. Chadwick et al., Nucl. Data Sheets **112**, 2887 (2011).

[6] K. Shibata et al., J. Nucl. Sci. Technol. **48**, 1 (2011).

[7] OECD/NEA Data Bank, "The JEFF-3.1.1 Nuclear Data Library", JEFF Report **22**, OECD/NEA Data Bank (2009).

[8] W.E. Kinney, J.W. McConnell, Int. Conf. on Interact. of Neutr. with Nuclei, Vol. **2** p. 1319 (1976).

[9] S.A. Cox, Prog: Argonne National Laboratory Report Series, No. **7210**, pp. 5 (1966).

[10] I.A. Korzh, V.A. Mishchenko, I.E. Sanzhur, Ukrainskii Fizishnii Zhurnal, Vol. **25**, Issue.1, pp. 109 (1980).

[11] D.J. Bredin, Physics Review, Vol. **135**, p. B412 (1964).

[12] R.L. Becker, W.G. Guindon, G.J. Smith, Nuclear Physics, Vol. **89**, pp.154 (1966).

[13] K. Tsukada, S. Tanaka, M. Maruyama, Y. Tomita, Reactor Physics Sem., Vol. **1**, pp.75 (1961).

[14] D.M. Drake, J.C. Hopkins, C.S. Young, H. Conde, A. Sattler, Nuclear Physics A, Vol. **128**, pp. 209 (1969).

[15] I.A. Korzh, N.S. Kopytin, M.V. Pasechnik, N.M. Pravdivy, N.T. Skijar, I.A. Tockij, Ukrainskii Fizichnii Zhurnal, Vol. **8**, p. 1323.

[16] G.A. Petitt, S.G. Buccino, C.E. Hollandsworth, P.R. Bevington, Nuclear Physics, Vol. **79**, pp. 231 (1966).

[17] S. Tanaka, K. Tsukada, M. Maruyama, Y. Tomita, Nuclear Data for Reactors Conf., Vol. **2**, p. 317 (1970).

[18] W.E. Kinney, F.G. Perey, Oak Ridge National Lab. Reports, No. **4517** (1970).

[19] J. Martin, D.T. Stewart, W.M. Currie, Nuclear Physics A, Vol. **113**, Issue 3, p. 564 (1968).

[20] D. Seeliger, D. Schmidt, T. Streil, Nuclear Physics A, Vol. **460**, p. 265 (1986).

[21] D. Schmidt, W. Mannhard, Jour. of Nuclear Science and Technology Suppl., Vol. **2**, Issue.1, p.226 (2002).

[22] C.R. Howell, R.S. Pedroni, G.M. Honore, K. Murphy, R.C. Byrd, G. Tungate, R.L. Walter, Physical Review C, Nuclear Physics, Vol. **38**, p.1552 (1988).

[23] Th. Schweitzer, D. Seeliger, K. Seidel, Kernenergie, Vol. **20**, p.174 (1977).

[24] H. -H. Knitter, M. Coppola, Zeitschrift f., Physik, Vol. **207**, p. 56 (1967).

[25] A.J. Koning, , S. Hilaire, M.C. Duijvestijn, in *Proceedings of the International Conference on Nuclear Data for Science and Technology*, France, 2007, edited by O.Bersillon, F.Gunsing, E.Bauge, R.Jacqmin, and S.Leray (2008), p. 211-214.

[26] J.R. Vanhoy, S.F. Hicks, H.E. Baber, B.P. Crider, E.E. Peters, F.M. Prados-Estévez, T.J. Ross, M.T. McEllistrem, and S.W. Yates, Proceedings of the AccApp13 Conference, Brugge, 5-8 August 2013.

[27] J.R. Vanhoy, Differential Cross Sections Measurements at the University of Kentucky Accelerator Adventures in Analysis, Tech. Rep. **13**, NEMEA-7 / CIELO, NEA/NSC/DOC (2014).

[28] J.R.Vanhoy, S.F.Hicks, A.Chakraborty, B.R.Champine, B.M.Combs, B.P.Crider, L.J.Kersting, A.Kumar, C.J.Lueck, S.H.Liu, P.J.McDonough, M.T.McEllistrem, E.E.Peters, F.M.Prados-Estevez, L.C.Sidwell, A.J.Sigillito, D.W.Watts, S.W.Yates, Nucl. Phys. A **939** (2015) 121.

[29] A.P.D. Ramirez, J.R. Vanhoy, S.F. Hicks, M.T. McEllistrem, E.E. Peters, S. Mukhopadhyay, T.D. Harrison, T.J. Howard, D.T. Jackson, P.D. Lenzen, T.D. Nguyen, R.L. Pecha, B.G. Rice, B.K. Thompson, and S.W. Yates, Phys. Rev. C **95**, 064605 (2017).

[30] P.E. Garret, N. Warr, and S. W. Yates, J. Res. Natl. Inst. Stand. Technol. **105**, 141 (2000), pp. 141-145.

[31] M. Drosg, Tech. Rep. IAEA-NDS-87 Rev. 8, IAEA, 2003.

[32] H. Liskien, A. Paulsen, At. Data Nucl. Data Tables **11** (7), 569 (1973).

[33] J. Lilley, Tech. Rep. P2N/934/80, Internal Service de Physique et Techniques Nucleaire, Centre

[34] X-5 Monte Carlo Team, Tech. Rep. LA-UR-13-22934, Los Alamos, National Laboratory, Apr. 2013.

[35] A.D. Carlson, V.G. Pronyaev, D.L. Smith, N.M. Larson, Z. Chen, G.M. Hale, F.-J. Hambsch, E.V. Gai, S.-Y, Oh, S.A. Badikov, T. Kawano, H.M. Hofmann, H. Vonach, S. Tagesen, Nucl. Data Sheets **110** (12) (2009) 3215.

[36] G.M. Hale, ENDF/V-II.1 ^{1}H(n,n) Reaction Evaluation, Tech. rep., LANL, Dec 2006.

[37] C.A. Engelbrecht, Nucl. Instrum. Methods **80** (2) (1970) 187.

[38] C.A. Engelbrecht, Nucl. Instrum. Methods **93** (1) (1971) 103.

[39] A. Negret, C. Borcea, Ph. Dessagne, M. Kerveno, A. Olacel, A.J.M. Plompen, M. Stanoiu, Phys. Rev. C **90** (2016) 034602.

[40] D. Dashdorj, G.E. Mitchell, J.A. Becker, U. Agvaanluvsan, L.A. Bernstein, W. Younes, P.E. Garrett, M.B. Chadwick, M. Devlin, N. Fotiades, T. Kawano, R. O. Nelson, Nuclear Science and Engineering **157** (2007), 65.

[41] A. Olacel, F. Belloni, C. Borcea, M. Boromiza, P. Dessagne, G. Henning, M. Kerveno, A. Negret, M. Nyman, E. Pirovano, A.J.M. Plompen, Phys. Rev. C **96**, 014621 (2017).

[42] S.P. Simakov, R. Capote, R.O. Nelson, V.G. Pronyaev, INDC(NDS)-0740 (2019).

[43] N. Otuka et al., Nucl. Data Sheets **120**, 272 (2014).

[44] L. Leal, N. Larson, D. Larson, D. Hetrick, Nuclear Data for Science and Technology, Int. Conf., Trieste, Italy.

[45] D. Hetrick, D. Larson, N. Larson, et al., Oak Ridge National Laboratory Report ORNL/TM-11825.

[46] A. Negret, C. Borcea, D. Bucurescu, D. Deleanu, Ph. Dessagne, D. Filipescu, D. Ghita, T. Glodariu, M. Kerveno, N. Marginean, R. Marginean, C. Mihai, S. Pascu, A.J.M. Plompen, T. Sava, L. Stroe, Phys. Rev. C **88**, 034604 (2013).

[47] M. Boromiza, C. Borcea, P. Dessagne, D. Ghita, T. Glodariu, G. Henning, M. Kerveno, N. Marginean, C. Mihai, R. Mihai, A. Negret, C. Nita, M. Nyman, A. Olacel, A. Oprea, A.J.M. Plompen, C. Sotty, G. Suliman, R. Suvaila, L. Stan, A. Turturica, and G. Turturica, Phys. Rev. C **101**, 024604 (2020).

[48] D. Lind and R. Day, Ann. of Phys **12**, 485-532 (1961).